CHEMISTRY OF MATERIALS
Article

Chem. Mater. **2009,** *21,* 5875–5885 5875
DOI:10.1021/cm902676d

Morphology and Refractive Index Sensitivity of Gold Island Films

Tanya Karakouz, Devora Holder, Mila Goomanovsky, Alexander Vaskevich,* and Israel Rubinstein*

Department of Materials and Interfaces, Weizmann Institute of Science, Rehovot 76100, Israel

Received August 30, 2009. Revised Manuscript Received November 5, 2009

The growing interest in recent years in gold island films prepared by vapor deposition on transparent substrates is largely attributed to the prominent localized surface plasmon (SP) extinction associated with nanostructured metal films. In the present study, two types of evaporated Au island films were investigated: (i) Au films (2.5, 5.0, and 7.5 nm nominal thickness) evaporated on silanized glass and annealed 20 h at a temperature <250 °C; (ii) Au films (7.5 and 10 nm nominal thickness) evaporated on unmodified glass and annealed 10 h at 550 or 600 °C. The 3D morphology of the Au islands was analyzed using high-resolution scanning electron microscopy (HRSEM), cross-sectional transmission electron microscopy (TEM), and atomic force microscopy (AFM) cross-sectional profilometry. Annealing at high temperatures, close to the glass transition temperature of the substrate, results in wetting of the Au islands by the glass and partial island embedding. The mechanism of morphology evolution during annealing changes from island coalescence and coarsening (low nominal thicknesses) to dewetting of percolated films (higher nominal thicknesses). The aspect ratio of more than 90% of the islands in annealed films is <1.5; therefore, splitting of the SP band to transversal and longitudinal components is not observed. The bulk refractive index sensitivity (RIS), in terms of SP wavelength shift and plasmon intensity change (PIC) per refractive index unit (RIU) change of the medium, was determined by measuring UV−vis spectra of Au island films in a series of methanol/chloroform mixtures. The RIS values for SP wavelength shift (RIS_{λ}) and PIC (RIS_{ext}) are 66−153 nm/RIU and 0.2−0.81 abs.u./RIU, respectively. The RIS shows a strong dependence on the wavelength of the SP maximum extinction, i.e., a higher RIS is measured for Au island films exhibiting a SP band at longer wavelengths. Partial thermal embedding of the Au islands in the glass substrate stabilizes the systems but lowers the RIS. The results presented may be useful for tuning the morphology and optical response of Au island films.

Introduction

Noble metal nanostructures supporting excitation of surface plasmon (SP) polaritons are of special interest in the rapidly developing nanotechnology. Interaction of electromagnetic radiation with noble metal (gold, silver) nanostructures (nanoparticles, island films, perforated continuous films, gratings) shows a localized SP resonance resulting in enhanced light scattering, a SP absorption band, and enhancement of the local electromagnetic field in the immediate environment.[1−3] The absorption maximum and intensity of the SP resonance band are sensitive to the size and shape of the nanostructures and the distance between them, as well as to the effective refractive index (RI) of the local surrounding environment.[1−3] The latter enables use of nanostructured noble metal films for detection and quantification of analyte binding to the metal surface by monitoring changes in the SP absorption band resulting from the local RI change. Localized surface plasmon resonance (LSPR) extinction bands of Ag and Au nanostructures are conveniently observed in the visible to near-IR part of the optical spectrum, allowing application of a variety of simple, well-developed setups of UV−vis transmission or reflection spectroscopy.[1−3] Leading platforms for the preparation of LSPR transducers include vacuum-evaporated ultrathin island or nanohole structured metal films and immobilized metal nanoparticles on transparent or reflecting substrates. Numerous studies have demonstrated chemical[2−5] and biological[2,3,6−13] sensing

*To whom correspondence should be addressed. E-mail: alexander.vaskevich@weizmann.ac.il (A.V.); israel.rubinstein@weizmann.ac.il (I.R.).

(1) Kreibig, U.; Vollmer, M. *Optical Properties of Metal Clusters*; Springer: Berlin 1995.
(2) Hutter, E.; Fendler, J. H. *Adv. Mater.* **2004**, *16*, 1685–1706.
(3) Stewart, M. E.; Anderton, C. R.; Thompson, L. B.; Maria, J.; Gray, S. K.; Rogers, J. A.; Nuzzo, R. G. *Chem. Rev.* **2008**, *108*, 494–521.
(4) Gluodenis, M.; Manley, C.; Foss, C. A., Jr. *Anal. Chem.* **1999**, *71*, 4554–4558.
(5) Okamoto, T.; Yamaguchi, I.; Kobayashi, T. *Opt. Lett.* **2000**, *25*, 372–374.
(6) Hutter, E.; Pileni, M.-P. *J. Phys. Chem. B* **2003**, *107*, 6497–6499.
(7) Larsson, E. M.; Alegret, J.; Kall, M.; Sutherland, D. S. *Nano Lett.* **2007**, *7*, 1256–1263.
(8) Marinakos, S. M.; Chen, S. H.; Chilkoti, A. *Anal. Chem.* **2007**, *79*, 5278–5283.
(9) Nath, N.; Chilkoti, A. *Anal. Chem.* **2004**, *76*, 5370–5378.
(10) Jonsson, M. P.; Dahlin, A. B.; Jonsson, P.; Höök, F. *Biointerphases* **2008**, *3*, FD30–FD40.
(11) Jonsson, M. P.; Jonsson, P.; Dahlin, A. B.; Höök, F. *Nano Lett.* **2007**, *7*, 3462–3468.
(12) Szunerits, S.; Praig, V. G.; Manesse, M.; Boukherroub, R. *Nanotechnology* **2008**, 19.
(13) Vaskevich, A.; Rubinstein, I. In *Handbook of Biosensors and Biochips*; Marks, R., Cullen, D., Lowe, C., Weetall, H. H., Karube, I., Eds.; Wiley: Chichester, 2007; Vol. *1*.

Published on Web 11/30/2009

using LSPR transducers, none of which, however, has been commercialized.

Major issues in the development of practical LSPR transducers include scalability of the preparation procedure, stability of the transducer structure and optical response, and sensitivity. We have extensively studied LSPR transducers based on Au island films on transparent substrates prepared by thermal evaporation and annealing, measured using transmission spectroscopy.[14−19] The film adhesion issue was tackled by evaporation of islands on a molecular adhesive layer of mercapto- or aminosilane[14,20] molecules or by partial embedding of the islands in the glass substrate induced by prolonged annealing at temperatures close to the glass transition temperature of the substrate.[19] Stabilization was also achieved by island encapsulation using an ultrathin (∼1−2 nm) layer of silica.[21]

Quantification of the LSPR transducer sensitivity is crucial for optimization as well as for comparison of different sensing platforms. Changes in the SP band wavelength,[5−8,11,22] the SP maximum extinction,[5,9,22] and complex parameters, which take into account the SP band shape,[22,23] have been used with LSPR transducers. In a realistic model[24] the two basic parameters determining the effectiveness of an LSPR system as an optical transducer are the refractive index sensitivity (RIS) and the decay length of the evanescent electromagnetic field. The RIS is commonly determined by measuring the optical extinction of the LSPR transducer upon immersion in a uniform bulk medium of variable RI, representing the bulk RIS. In a typical LSPR sensor, an analyte of a certain size binds to a recognition layer on the LSPR transducer, effecting a local change of the RI. The finite thicknesses of the analyte and recognition layers can be taken into account using the bulk RIS and assuming an exponential decay of the electromagnetic field with a characteristic decay length, presenting a simple, two-parameter model providing a quantitative description of the system.[24]

The RIS presents a characteristic value for the upper limit of the response of a given LSPR transducer to refractive index change, comprising necessary data for evaluation of the system performance. RIS measurements have been reported for a variety of systems, including metal nanoparticles and nanorods in solution[7,25] and immobilized on substrates,[8,9,26−28] nanoholes in thin, continuous metal films,[11] and metal island arrays evaporated through a mask.[29−31] Data for random Au island films are rather limited.[4,12,32−35]

Our used method of vacuum evaporation of a metal film combined with thermal annealing presents a simple and scalable preparation scheme for LSPR transducers, while variation of the conditions (evaporation rate, mass thickness of the film, annealing temperature and time, chemical modification of the substrate) provides control over the film morphology and optical properties. Here, we present a systematic study of the morphology and RIS of Au island films on aminosilane-modified glass[21] (nominal thickness: 2.5, 5.0, 7.5 nm) and on bare glass in which the islands are partially embedded[19] (nominal thickness: 7.5, 10 nm). The thickness range was chosen to enable obtaining a series of Au island system of different morphologies and optical properties using evaporation and moderate annealing. The structures are analyzed using high-resolution scanning electron microscopy (HRSEM), cross-sectional transmission electron microscopy (TEM), and atomic force microscopy (AFM) cross-sectional profilometry, offering a detailed characterization of the 3D shape of the Au islands. Cross-sectional images of Au islands partially embedded in the glass substrate, obtained using focused ion beam (FIB) slicing and TEM imaging, indicate that the embedding mechanism involves wetting of the islands by the softened glass.

The present study identifies general trends relating film morphology, spectroscopic properties, and RIS. Due to the statistical nature of the ensembles of Au islands, presenting a distribution of sizes and shapes, as well as different interactions with the glass (aminosilane vs embedding), connection between these parameters and the RIS of the LSPR transducers has to be determined experimentally. The present results show a correlation between the aspect ratio of the Au islands and the full width at half-maximum (fwhm) of the SP band. An analytical model considering a linear dependence of the real part of the Au dielectric constant on the wavelength

(14) Doron-Mor, I.; Barkay, Z.; Filip-Granit, N.; Vaskevich, A.; Rubinstein, I. *Chem. Mater*. **2004**, *16*, 3476–3483.
(15) Doron-Mor, I.; Cohen, H.; Barkay, Z.; Shanzer, A.; Vaskevich, A.; Rubinstein, I. *Chem.—Eur. J*. **2005**, *11*, 5555–5562.
(16) Kalyuzhny, G.; Schneeweiss, M. A.; Shanzer, A.; Vaskevich, A.; Rubinstein, I. *J. Am. Chem. Soc*. **2001**, *123*, 3177–3178.
(17) Kalyuzhny, G.; Vaskevich, A.; Ashkenazy, G.; Shanzer, A.; Rubinstein, I. *J. Phys. Chem. B* **2000**, *104*, 8238–8244.
(18) Kalyuzhny, G.; Vaskevich, A.; Schneeweiss, M. A.; Rubinstein, I. *Chem.—Eur. J*. **2002**, *8*, 3849–3857.
(19) Karakouz, T.; Tesler, A. B.; Bendikov, T. A.; Vaskevich, A.; Rubinstein, I. *Adv. Mater*. **2008**, *20*, 3893–3899.
(20) Bendikov, T. A.; Rabinkov, A.; Karakouz, T.; Vaskevich, A.; Rubinstein, I. *Anal. Chem*. **2008**, *80*, 7487–7498.
(21) Ruach-Nir, I.; Bendikov, T. A.; Doron-Mor, I.; Barkay, Z.; Vaskevich, A.; Rubinstein, I. *J. Am. Chem. Soc*. **2007**, *129*, 84–92.
(22) Dahlin, A. B.; Tegenfeldt, J. O.; Höök, F. *Anal. Chem*. **2006**, *78*, 4416–4423.
(23) Schmitt, J.; Machtle, P.; Eck, D.; Mohwald, H.; Helm, C. A. *Langmuir* **1999**, *15*, 3256–3266.
(24) Jung, L. S.; Campbell, C. T.; Chinowsky, T. M.; Mar, M. N.; Yee, S. S. *Langmuir* **1998**, *14*, 5636–5648.
(25) Chen, H. J.; Kou, X. S.; Yang, Z.; Ni, W. H.; Wang, J. F. *Langmuir* **2008**, *24*, 5233–5237.
(26) Nath, N.; Chilkoti, A. *Anal. Chem*. **2002**, *74*, 504–509.
(27) Sun, Y. G.; Xia, Y. N. *Anal. Chem*. **2002**, *74*, 5297–5305.
(28) Ni, W.; Chen, H.; Kou, X.; Yeung, M. H.; Wang, J. *J. Phys. Chem. C* **2008**, *112*, 8105–8109.
(29) Jensen, T. R.; Duval, M. L.; Kelly, K. L.; Lazarides, A. A.; Schatz, G. C.; Van Duyne, R. P. *J. Phys. Chem. B* **1999**, *103*, 9846–9853.
(30) Malinsky, M. D.; Kelly, K. L.; Schatz, G. C.; Van Duyne, R. P. *J. Am. Chem. Soc*. **2001**, *123*, 1471–1482.
(31) Hicks, E. M.; Zhang, X. Y.; Zou, S. L.; Lyandres, O.; Spears, K. G.; Schatz, G. C.; Van Duyne, R. P. *J. Phys. Chem. B* **2005**, *109*, 22351–22358.
(32) Szunerits, S.; Das, M. R.; Boukherroub, R. *J. Phys. Chem. C* **2008**, *112*, 8239–8243.
(33) Meriaudeau, F.; Downey, T. D.; Passian, A.; Wig, A.; Ferrell, T. L. *Appl. Opt*. **1998**, *37*, 8030–8037.
(34) Hanarp, P.; Kall, M.; Sutherland, D. S. *J. Phys. Chem. B* **2003**, *107*, 5768–5772.
(35) Zheng, Y. B.; Juluri, B. K.; Mao, X. L.; Walker, T. R.; Huang, T. J. *J. Appl. Phys*. **2008**, 103.

in the spectral region 500−800 nm predicts a linear dependence of the RIS on the SP wavelength.[36,37] The experimental data are in agreement with this model, showing the expected correlation between the two parameters. The empirical correlation between the RIS and SP band wavelength enables estimation of the RIS for different LSPR systems using transmission spectra measurements.

Experimental Section

Chemicals. Chloroform (BioLab), ethanol (Baker analyzed, J.T. Baker), methanol (anhydrous, Mallinckrodt chemicals), sulfuric acid (H_2SO_4) (95−98%, BioLab), hydrogen peroxide (H_2O_2) (30%, Frutarom), ammonium hydroxide (NH_4OH) (Frutarom), 3-aminopropyl trimethoxysilane (APTS) (Aldrich), and Au (99.99%, Holland-Moran, Israel) were used as received. Water was triply distilled. The inert gas used was household nitrogen (from liquid N_2).

Gold Island Film Preparation. Two types of Au island films were prepared as described previously: Au films evaporated directly on glass (high-temperature annealed Au island films)[19] and Au films evaporated on glass precoated with an organic adhesion layer (low-temperature annealed Au island films).[20] Microscope cover glass slides (Menzel-Gläser, No. 3), cut to 22×9 mm^2, were used as substrates for both types of films.

High-Temperature Annealed Au Island Films. The glass slides were cleaned by immersion in freshly prepared hot piranha solution (1:3 H_2O_2/H_2SO_4) for 1 h followed by rinsing with triply distilled water, rinsing in ethanol three times in an ultrasonic bath (Cole-Parmer 8890), and drying under a steam of nitrogen. (*Caution: Piranha solution reacts violently with organic materials and should be handled with extreme care.*) After cleaning, the slides were mounted in a cryo-HV evaporator (Key High Vacuum) equipped with a Maxtek TM-100 thickness monitor for evaporation of ultrathin Au films. Homogeneous Au deposition was obtained by moderate rotation of the substrate plate. Au (nominal thickness, 7.5 and 10 nm) was resistively evaporated from a tungsten boat at $1-3 \times 10^{-6}$ torr at a deposition rate of 0.005−0.006 nm s^{-1} (determined by measuring the evaporation time of 0.1 nm Au using a stopwatch). Postdeposition annealing of Au-coated slides was carried out in air at 550 or 600 °C for 10 h in an oven (Ney Vulcan 3−550). The heating rate was 5 °C min^{-1}, and the annealed slides were left to cool to room temperature in air.

Low-Temperature Annealed Au Island Films. The glass slides cleaned with piranha solution (see above) and rinsed with triply distilled water were immersed in "RCA" solution (1:1:5 $H_2O_2/NH_4OH/H_2O$) for 1 h at 70 °C, followed by rinsing with triply distilled water and rinsing in methanol three times in an ultrasonic bath. After being cleaned, the slides were silanized by immersion in 10% APTS solution in methanol overnight, followed by rinsing with methanol and twice with ethanol in the ultrasonic bath.[38] Au island films (nominal thickness, 2.5, 5.0, and 7.5 nm) were resistively evaporated under the conditions described above for high-temperature annealed Au island films. Postdeposition annealing of Au-coated slides was carried out in the oven in air at different temperatures ranging from 100 to 250 °C. The annealing time varied from 2.5 to 40 h. The heating rate was 5 °C min^{-1}, and the annealed slides were left to cool in air to room temperature.

Preparation of Slices for Cross-Sectional Transmission Electron Microscopy (TEM). Samples of low-temperature annealed Au films were embedded in a phenol-based M-Bond 610 epoxy resin (Ted Pella Inc., Redding, CA) according to a procedure described previously[39] with some modifications. The Au island film was glued with several drops of the resin onto a premade 4×8 mm^2 block of the epoxy. (The resin solution was cast in a rubber mold (Structure Probe Inc., West Chester, PA) and cured 3 days at 80 °C.) The glass substrate was removed by breaking it off the Au film or by dissolving it in diluted (∼5%) HF solution. The backside of the Au was covered with several drops of the resin solution. The epoxy resin was cured 3 days at 80 °C. The embedded samples were then sectioned into thin (30−50 nm) slices using a diamond knife (Micro Star 45°) and a Leica ULTRACUT UCT Ultramicrotome. The samples were sliced perpendicular to the surface of the sample and placed on carbon/collodion-coated copper grids.

Cross-section samples of high-temperature annealed Au films were prepared using FEI Strata 400S dual-beam focused ion beam (FIB) microscope using the "lift-out" technique. The Au island film on glass was coated by ∼70−80 nm Cr followed by 2−3 μm Pt (the latter was partially removed during lamella thinning) to reduce image drift due to charging and to prevent ion damage to the surface. The accelerating voltage and current of the incident e-beam were maintained at 5 kV and 1.6 nA, respectively, throughout the entire process. A lamella (∼12 × 8x2 μm) was formed by milling with the ion beam (accelerating voltage, 30 kV; ion current, 2.8 nA to 48 pA). The lamella was then lifted from the substrate and attached to the TEM grid using a nanomanipulator (Omniprobe, AutoProbe 200). Final polishing of the lamella was performed at 5 kV and 10 pA, followed by cleaning at 2 kV and 1.6 pA to eliminate ion beam induced damage from the previous stages. The final thickness of the cross section was estimated as 50−100 nm.

Determination of the Bulk RIS. Test solutions with variable refractive index (RI) in the range 1.327 to 1.445 were prepared by mixing methanol ($n = 1.327$) and chloroform ($n = 1.445$) at different ratios (1:0; 1:3; 1:1; 3:1; 0:1). The RI of the solutions was determined using an Abbe refractometer. Transmission UV−vis spectra were measured with the slide placed in a quartz cuvette filled with a solution of a given RI. The same solution in the quartz cuvette was measured as baseline before insertion of the sample. The measurements were carried out after performing a stabilization procedure, i.e., dipping the sample in ethanol and drying under a stream of nitrogen several times until no change in the extinction spectrum was observed.[40] The stability of the optical response was tested by carrying out the measurements sequentially in solutions with ascending and descending RI values.

Characterization Methods. *UV−Vis Spectroscopy.* Transmission spectra of thin films were obtained with a Varian CARY 50 spectrophotometer. The measurement parameters were as follows: wavelength resolution, 1 nm; average acquisition time per point, 0.1 s. The spectra were measured using a special slide holder ensuring reproducible position of the sample.[17]

(36) Miller, M. M.; Lazarides, A. A. *J. Phys. Chem. B* **2005**, *109*, 21556–21565.
(37) Lee, K. S.; El-Sayed, M. A. *J. Phys. Chem. B* **2006**, *110*, 19220–19225.
(38) Wanunu, M.; Vaskevich, A.; Rubinstein, I. *J. Am. Chem. Soc.* **2004**, *126*, 5569–5576.
(39) Wanunu, M.; Popovitz-Biro, R.; Cohen, H.; Vaskevich, A.; Rubinstein, I. *J. Am. Chem. Soc.* **2005**, *127*, 9207–9215.
(40) The high-temperature annealed Au island films do not show change in the UV−vis spectra after the first immersion in ethanol and drying.

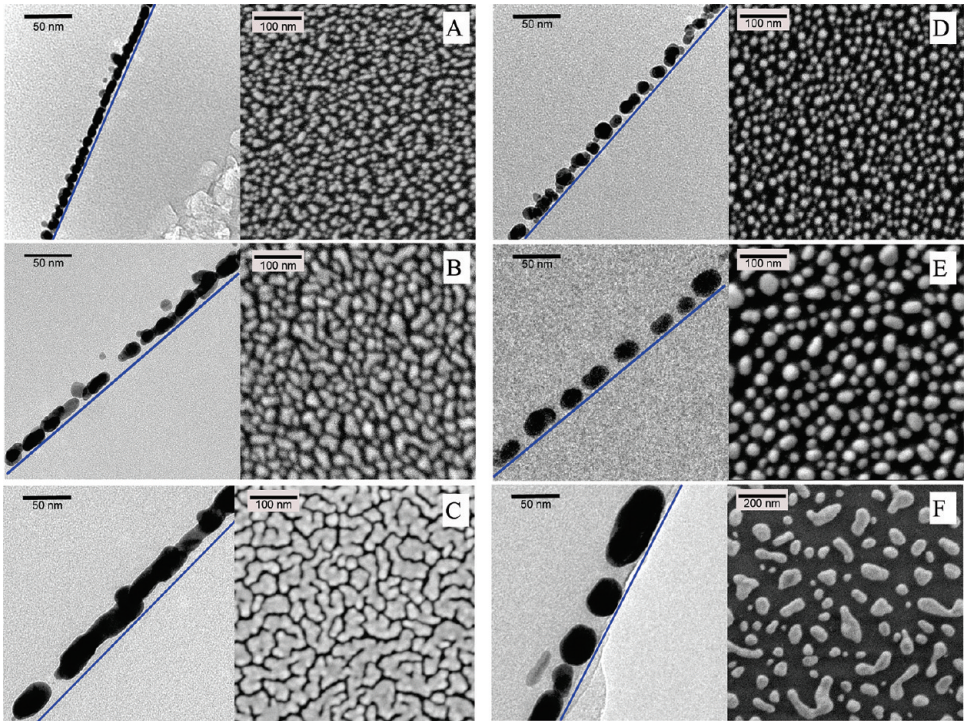

Figure 1. Cross-sectional TEM (left panels) and HRSEM (right panels) images of gold films evaporated on silanized glass. Nominal thickness: 2.5 nm (A, D), 5.0 nm (B, E), and 7.5 nm (C, F). Samples before (A, B, C) and after (D, E, F) annealing 20 h at 200 °C are shown. The solid lines in the cross-sectional TEM images serve as a guide to the eye, representing the glass substrate removed before sectioning. Note the different scale bar in (F).

High-Resolution Scanning Electron Microscopy (*HRSEM*). HRSEM images were obtained using the SE detector in an ULTRA 55 FEG ZEISS high-resolution SEM. The measurements were carried out at an applied voltage of 2 kV and a working distance of 3 mm.

Cross-Sectional Transmission Electron Microscopy (*TEM*). TEM images were acquired using a Philips CM-120 transmission electron microscope operating at 120 kV, equipped with a charge-coupled device (CCD) camera (2kx2k, Gatan Ultrascan 1000).

Atomic Force Microscopy (*AFM*). AFM measurements were carried out in air using a molecular imaging (MI) PicoScan instrument operating in the acoustic AC mode. The cantilevers used were NSC35 or NSC36 series of ultrasharp silicon (MikroMasch, Estonia) with a resonant frequency of 75−150 kHz and an average radius of ≤10 nm.

Results and Discussion

Morphology of Evaporated Au Films. Ultrathin Au island films of 2.5, 5.0, and 7.5 nm (mass thickness) were evaporated on silanized glass and annealed in air. Annealing temperatures of < 250 °C were chosen to preserve the adhesion provided by the organic intermediate layer; in most low-temperature experiments, the annealing was carried out at 200 °C.[14,41] Figure 1 presents HRSEM and cross-sectional TEM images of Au island films, unannealed and annealed 20 h at 200 °C. The unannealed islands present a rather complex shape, reflecting concurrent accumulation of Au on the substrate surface and coalescence of primary nucleated islands during evaporation. Reshaping of the Au islands during annealing, driven by capillary forces, coalescence, and Ostwald ripening, proceeds on the time scale of tens of hours due to the slow surface diffusion at 200 °C. After 2.5 h of annealing, most islands in a 5 nm-thick Au film retain the irregular shape, whereas after 5 h they become mostly concave (not shown). Longer annealing results in gradual increase of the average island size. The usual annealing time was set to 20 h, when the area fraction covered by Au islands stabilizes.

As seen from Figure 1A−C, the increase in the nominal thickness of the unannealed films leads to enlargement of the islands, eventually forming a near-percolated film at 7.5 nm. Annealing of 2.5 and 5.0 nm Au films produces ensembles of islands presenting a regular shape, from round to elliptical (Figure 1D,E), while the annealed 7.5 nm film shows elongated and wormlike island shape (Figure 1F). The latter reflects the relatively slow reshaping of islands, following formation of a neck between adjacent islands, attributed to the low diffusion coefficient and limited mobility of grain boundaries at 200 °C. The annealing leads to an increase in the average size of individual islands and of the average distance between islands, in agreement with our previous results on Au island films evaporated on glass precoated with a mercaptosilane layer.[14]

The island shape and average vertical dimension were obtained from cross-sectional TEM images (Figure 1). The annealed films present larger and more spaced Au islands compared with the unannealed films. The slices (30−50 nm thick) of the unannealed samples contain more than one row of islands, while images of the annealed films show separated individual islands.

(41) Goss, C. A.; Charych, D. H.; Majda, M. *Anal. Chem.* **1991**, *63*, 85–88.

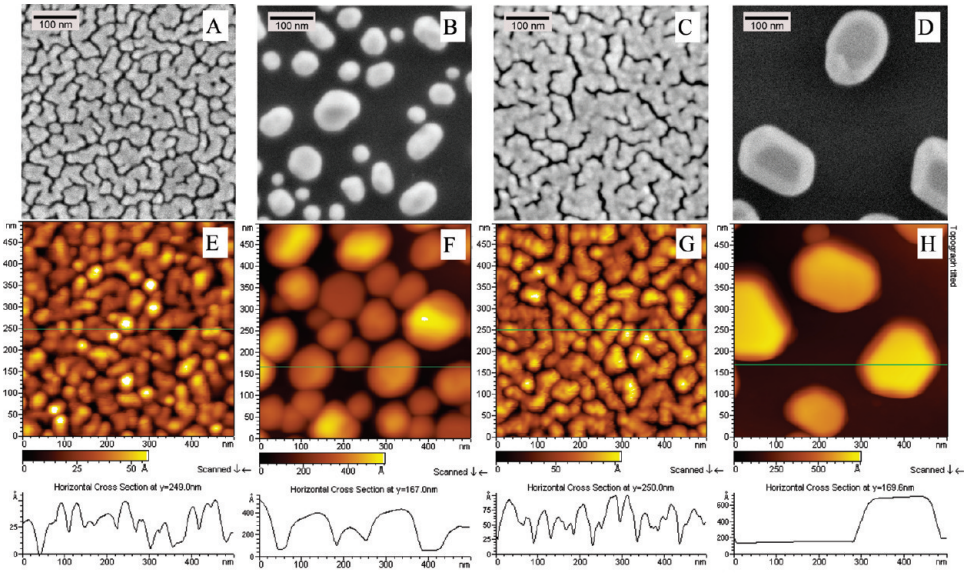

Figure 2. HRSEM (A−D) and AFM (E−H) images of gold films evaporated on bare glass. Nominal thickness: 7.5 nm (A, B, E, F) and 10 nm (C, D, G, H). Samples before (A, C, E, G) and after (B, D, F, H) annealing 10 h at 550 °C are shown. A typical cross section is shown below each AFM image; note the different z-scales in the cross sections.

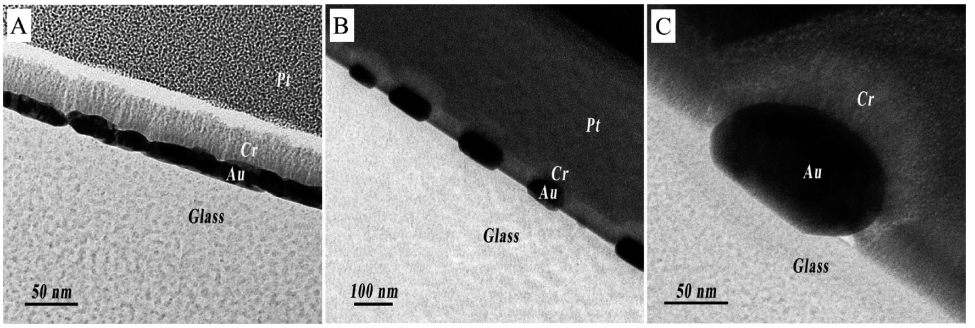

Figure 3. Cross-sectional TEM images of 10 nm gold films evaporated on bare glass. Sample before (A) and after (B, C) high-temperature annealing (10 h at 600 °C) are shown. The samples were prepared by focused ion beam (FIB) slicing (see Experimental Section).

We have recently introduced highly stable Au island films prepared by evaporation on unmodified glass substrates (no adhesion layer) followed by prolonged annealing in air at 550−650 °C, resulting in partial embedding of the Au islands in the glass.[19] Transformation of the morphology from percolated to separated islands was followed by AFM and HRSEM (Figure 2) and by cross-sectional TEM (Figure 3). As seen in Figure 3C, the softened glass wets the embedded Au island. The same kind of behavior was observed with Au nanoparticles immobilized on glass and annealed at similar temperatures.[42,43] Recently, wetting of Au islands on sapphire by an intermediate liquid anorthite layer was shown.[44] In the latter case, a nanometer-thick amorphous layer of anorthite separated the Au islands and the sapphire surface, forming an intergranular film at the interface.[44] In the present system, additional studies of the chemical composition of the interface are necessary to elucidate the mechanism of Au island embedding in the softened glass.

The unannealed 7.5 and 10 nm films show a largely percolated structure with a network of voids; the latter becoming shorter as the nominal thickness is increased (Figure 2A,C,E,G). As noted above for the thinner films, the cross-sectional TEM image (Figure 3A) shows overlap of Au grains in the sliced film. High-temperature annealing of the near-percolated 7.5 and 10 nm films leads to formation of large, well-separated islands (Figure 2B,D,F,H). Selected-area electron diffraction shows that the individual islands are single crystalline.[45] The top surface of larger faceted islands formed after annealing of 10 nm films is more developed, as seen in the HRSEM and AFM images (Figure 2D,H). The AFM measured roughness of the top surface of the annealed films is ca. 0.1 nm over a 100 nm scan, indicating largely atomically flat surfaces. XRD analysis of high-temperature annealed 10 nm Au films shows a strong {111} texture,[45] confirming that the top surfaces

(42) Natan, M. J.; Reiss, B. D.; Keefe, M. H. Thermal Immobilization of Colloidal Metal Nanoparticles in a Glass Matrix. 2000-US32854 2001040132, Dec. 04, **2000**.
(43) Karakouz, T.; Vaskevich, A.; Rubinstein, I. Weizmann Institute of Science, Rehovot, Israel, 2009; unpublished results.
(44) Baram, M.; Kaplan, W. D. *J. Mater. Sci.* **2006**, *41*, 7775–7784.
(45) Tesler, A. B.; Karakouz, T.; Maoz, B.; Feldman, I.; Vaskevich, A.; Rubinstein, I., in preparation.

Table 1. Statistical Analysis (Mean Value ± Standard Deviation) of Annealed Gold Island Films

nominal thickness (nm)	annealing temperature (°C)/time (h)	a^a (nm)	b^a (nm)	c^b (nm) TEM	c^b (nm) AFM	aspect ratio (a/b)	Feret diameter (nm)	equivalent diameter (nm)	top-view area (nm^2)
Low-Temperature Annealed Au Island Films Evaporated on Silanized Glass									
2.5	200/20	13 ± 5	10 ± 4	13 ± 2		1.30 ± 0.27	16 ± 5	13	130 ± 80
5	200/20	27 ± 10	21 ± 6	22 ± 6		1.30 ± 0.22	28 ± 9	24	447 ± 255
7.5	200/20			39 ± 8			88 ± 55	68	3602 ± 3355
High-Temperature Annealed Au Island Films Evaporated on Bare Glass									
7.5	550/10	54 ± 17	44 ± 12		30 ± 8	1.25 ± 0.19	59 ± 20	53	2235 ± 1420
10	550/10	139 ± 44	110 ± 31		49 ± 15	1.30 ± 0.23	146 ± 50	131	13454 ± 8213
10	600/10	138 ± 57	105 ± 42	63 ± 18	41 ± 13	1.30 ± 0.28	140 ± 46	125	12240 ± 7101

[a] a: island length; b: island width, both measured from HRSEM images. [b] c: island height.

of individual Au islands (Figures 2D,H and 3) present (111) faces.

The combination of HRSEM and cross-sectional TEM imaging allows quantitative determination of the 3D island shape obtained for different film thicknesses and annealing conditions. Measurements of island lateral dimensions were carried out using ImageJ software[46] on HRSEM images. Average values of the following island parameters were determined for samples of 350 islands: a, length; b, width; d_F, Feret diameter, i.e., the maximum chord (maximum caliper distance) across the island;[47] S, top-view island area; d_e, equivalent diameter, i.e., the diameter of a circle whose area equals the island top-view area; $d_e = (4S/\pi)^{0.5}$. Island height (c) was measured manually from cross-sectional TEM images of an ensemble of 100 islands (low-temperature annealed islands) and AFM images of 100 islands or cross-sectional TEM images of 42 islands (high-temperature annealed islands). AFM was not used for height measurements of low-temperature annealed islands due to the higher island density and possible tip convolution. Average values of island dimensions are summarized in Table 1.

Dissolution of high-temperature annealed Au island films in aqua regia reveals depressions in the glass resulting from partial embedding of the islands in the glass. The depth of embedding increases with the annealing temperature, from 1.5 ± 0.5 nm at 550 °C to 9.0 ± 2.0 nm at 600 °C.[19] The more pronounced island embedding is also seen as a decrease of ca. 8 nm in Au island height measured by AFM profilometry (Table 1). The island height above the glass substrate, measured from cross-sectional TEM images (Figure 3), gives a value of 46 ± 16 nm, which is similar within the statistical error to that determined by AFM. However, the island embedding depth of 18 ± 8 nm obtained from the cross-sectional TEM images is larger than that measured by AFM.[19] The origin of this deviation, as well as the nature of the glass−island interface following high-temperature annealing, require further study.

Shape−size relationship for Au island samples was analyzed using scattering diagrams, comparing the Feret diameter and the equivalent diameter (Figure 4). Deviation of the experimental data in the scattering field from the straight line $d_F = d_e$ is a measure of island noncircularity. The correlation fields of low-temperature annealed 2.5 and 5.0 nm films overlap within the experimental error, showing moderate deviation from circularity (see inset in Figure 4A). The island shape can be approximated as a lying prolate ellipsoid ($a > b \approx c$, Table 1). The correlation field for low-temperature annealed 7.5 nm film overlaps with the data for 2.5 and 5.0 nm films in the region $d_e < 40$ nm, while for $d_e > 40$ nm a marked deviation and increase in the data scatter are seen (Figure 4A).

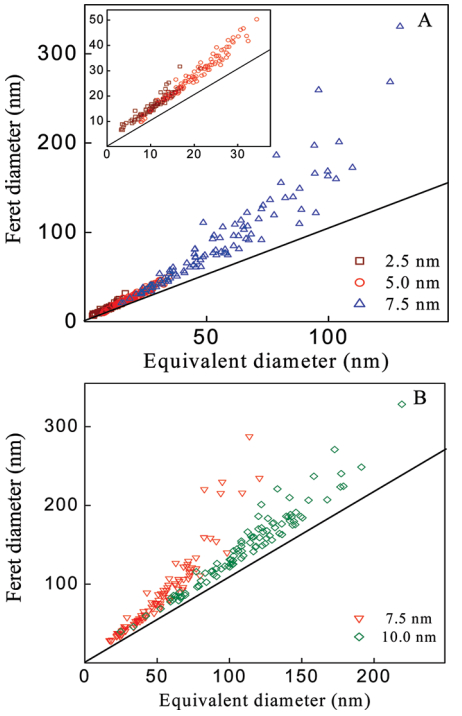

Figure 4. Correlation between the Feret diameter d_F and the equivalent diameter d_e of annealed Au island films. (A) Au films after low-temperature annealing (20 h at 200 °C); inset: zoom on the 2.5 and 5.0 nm films. (B) Au films after high-temperature annealing (10 h at 550 °C). Nominal thicknesses are indicated. Mean island dimensions were calculated from HRSEM images of Au island films using ImageJ program. The straight lines correspond to $d_F = d_e$.

The scattering field of the high-temperature annealed 7.5 nm film shows a larger deviation from circularity

(46) Rasband, W. National Institute of Health, USA; ImageJ 1.29x; http://rsb.info.nih.gov/ij.
(47) Walton, W. H. *Nature* **1948**, *162*, 329–330.

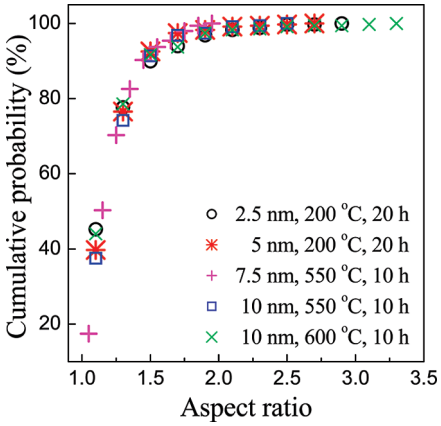

Figure 5. Cumulative probability of the aspect ratio of annealed Au islands. Aspect ratio values were calculated from HRSEM images of Au island films using ImageJ program. Film nominal thicknesses and annealing regimes are indicated.

compared to that of the 10 nm film (Figure 4B). The scatter of the experimental data for the high-temperature annealed 7.5 film (Figure 4B) increases with d_e in a qualitatively similar manner to that of the low-temperature annealed 7.5 nm film (Figure 4A). The statistical data in Table 1 indicate that the Au island shape obtained after high-temperature annealing of 7.5 and 10 nm films deviates from prolate ellipsoid. We assume that the large scatter observed in the d_F-d_e correlation field for both low- and high-temperature annealed 7.5 nm films reflects the mechanism of island thermal reshaping. Unannealed 7.5 nm films are near-percolated, showing no DC electrical conductivity; however, island clusters with lateral dimensions larger than the mean distance between voids are already interconnected (Figures 1C and 2A). The mechanism of shape transformation of such films during annealing is complex, combining island coalescence and dewetting. On the other hand, unannealed 2.5 and 5.0 nm films consists of separated islands (Figure 1A,B); therefore, island movement and coalescence combined with Ostwald ripening present the major mechanisms of morphology transformation during annealing. Unannealed 10 nm films are fully percolated and electrically conducting (Figure 2C), hence the annealing induces dewetting of the continuous structure and island formation.[45]

Mean values (Table 1) and statistical distribution (Figure S1 in the Supporting Information) of the Au island aspect ratio were obtained for all thicknesses and annealing regimes except the 7.5 nm low-temperature annealed films, where irregular u-shaped islands comprise a substantial fraction of the ensemble (Figure 1F). The cumulative probability (Figure 5) and histograms (Figure S1 in the Supporting Information) indicate that in all films more than 90% of all islands have an aspect ratio lower than 1.5.

Optical Properties of Au Island Films. Typical transmission UV−vis spectra of Au films before and after annealing are presented in Figures 6 and 7. Unannealed films presenting an island structure (small nominal thicknesses, 2.5 and 5.0 nm) show a well-defined SP band in the visible spectral range. Evolution of the spectra upon thermal

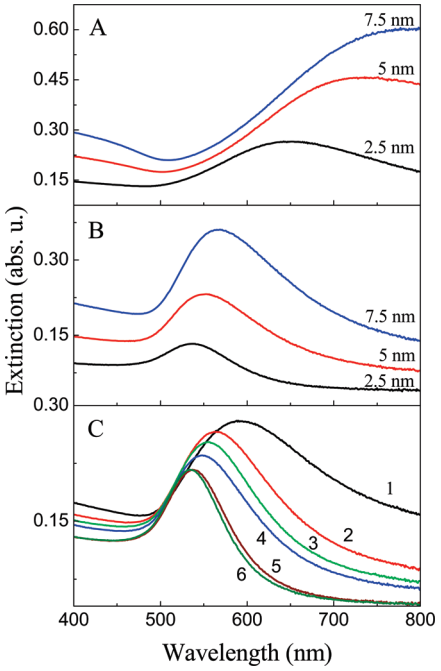

Figure 6. Transmission UV−vis spectra of Au films evaporated on silanized glass. (A) As evaporated; (B) after annealing 20 h at 200 °C; nominal thicknesses in A and B are indicated. (C) 5 nm Au film after annealing 20 h at the following temperatures: 1, 100 °C; 2, 150 °C; 3, 175 °C; 4, 200 °C; 5, 225 °C; 6, 250 °C.

annealing is in agreement with the well-known optical properties of thin Au films.[4,14,18] The blue shift of the SP band maximum following low-temperature annealing (Figure 6B) is attributed to decoupling of SPs due to the increase in the interisland spacing (Figure 1A,B,D,E). The blue shift increases with the annealing temperature (Figure 6C).

The SP band is barely distinguishable in the spectra of the 7.5 nm unannealed films (Figures 6A and 7A), approaching the spectrum of a continuous Au film, in agreement with the HRSEM imaging results (Figures 1C and 2A). The unannealed 10 nm film is highly electronically conductive and exhibits a transmission UV−vis spectrum (Figure 7A) characteristic of a continuous Au film, showing an extinction minimum at ca. 520 nm and the absence of a SP band.[48] High-temperature annealing transforms the percolated Au films to isolated islands, resulting in the appearance of a well-defined SP band (Figure 7).

Transmission spectra of Au nanorods with aspect ratios >2 were shown to display two clearly resolved SP bands, transversal and longitudinal.[49−51] When the nanorod aspect ratio was 1.5, the two bands were not separated, showing substantial broadening of the SP extinction peak.[52] Increase of the aspect ratio to

(48) Norrman, S.; Andersson, T.; Granqvist, C. G.; Hunderi, O. *Phys. Rev. B* **1978**, *18*, 674–695.
(49) Khlebtsov, N. G. *Quantum Electron.* **2008**, *38*, 504–529.
(50) Link, S.; El-Sayed, M. A. *J. Phys. Chem. B* **1999**, *103*, 8410–8426.
(51) Murphy, C. J.; San, T. K.; Gole, A. M.; Orendorff, C. J.; Gao, J. X.; Gou, L.; Hunyadi, S. E.; Li, T. *J. Phys. Chem. B* **2005**, *109*, 13857–13870.
(52) Sprunken, D. P.; Omi, H.; Furukawa, K.; Nakashima, H.; Sychugov, I.; Kobayashi, Y.; Torimitsu, K. *J. Phys. Chem. C* **2007**, *111*, 14299–14306.

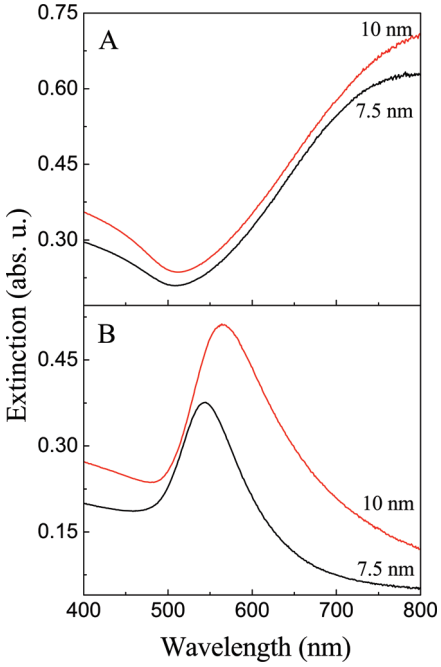

Figure 7. Transmission UV−vis spectra of gold films evaporated on bare glass, before (A) and after (B) annealing 10 h at 550 °C. Nominal thicknesses are indicated.

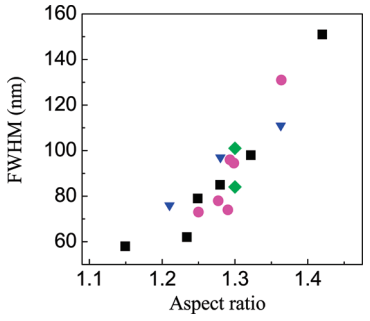

Figure 8. Relationship between the fwhm of the SP band and the average aspect ratio of Au islands in annealed films. Squares: 5 nm Au film evaporated on silanized glass, annealed 20 h at different temperatures; circles: 5 nm Au film evaporated on silanized glass, annealed at 200 °C for different times; diamonds: Au films of different thicknesses evaporated on silanized glass, annealed 20 h at 200 °C; triangles: Au films of different thicknesses evaporated on bare glass, annealed 10 h at 550 °C.

1.8 caused further broadening of the extinction peak and the appearance of two overlapping SP band maxima.[53] These experimental observations are in agreement with calculation of the evolution of a Au nanorod spectrum as a function of aspect ratio.[49] In the present work, extinction spectra of island films formed after annealing (Figures 6 and 7) do not show splitting of the SP band, as only a small fraction of the islands, less than 2%, can be defined as "nanorods" with an aspect ratio ≥2.0 (Figure 5). The effect of aspect ratio on band broadening is presented in Figure 8 as the relationship between the full width at half-maximum (fwhm) of the SP band and the mean aspect ratio. Although the fwhm also depends on the size of the Au nanostructures (see Table 2),[50,54] the influence of the aspect ratio on the fwhm is evident as a common correlation for different Au island films (Figure 8).

Table 2. Characteristic Average Parameters of Annealed Gold Island Films

nominal thickness (nm)	annealing temperature (°C)	SP band wavelength[a] (nm)	fwhm (nm)	RIS_λ (nm/RIU)	RIS_{ext} (abs.u./RIU)	FOM (RIS_λ/fwhm)
Low-Temperature Annealed Au Island Films						
2.5	200	536	84	66	0.20	0.786
5	200	552	101	80	0.36	0.792
7.5	200	566	114	121	0.54	1.061
High-Temperature Annealed Au Island Films						
7.5	550	544	76	93	0.81	1.224
10	550	565	97	153	0.67	1.577
10	600	587	111	114	0.23	1.027

[a] Measured in air.

Reproducibility of the LSPR transducer preparation procedure is critical in the development of practical sensors. The standard deviation of the nominal thickness of slides evaporated in the vacuum chamber with a rotating holder is ≤4%, attesting to the homogeneity of the evaporated batch of slides.[55] Statistical analysis of extinction spectra was carried out using six batches of 18−24 slides each, nominal thicknesses of 2.5 to 10 nm, and different annealing procedures. The standard deviation of the SP band wavelength for a given batch varied between 1 and 4 nm, with an average of 2.3 nm, while the relative standard deviation of the SP maximum extinction was ≤2%. The statistical data show that thermal evaporation of thin Au films followed by annealing presents a viable route to large-scale preparation of LSPR transducers.

Refractive Index Sensitivity (RIS) of Au Island Films. The bulk RIS of the Au films was evaluated by measuring extinction spectra of annealed samples immersed in a series of methanol−chloroform mixtures with refractive indexes in the range from 1.327 (pure methanol) to 1.445 (pure chloroform) (Figure 9). All the Au island films were stable when exposed to the organic solvents: The measurements were carried out by increasing the chloroform−methanol ratio from pure methanol to pure chloroform and then decreasing back to pure methanol, producing perfectly overlapping spectra, as seen in Figure 9. The increase in the refractive index of the surrounding medium results in a red shift of the SP band, in agreement with the Maxwell-Garnett effective medium theory.[56]

In various reported cases, such as Ag island arrays prepared by colloidal lithography,[29,30] while the shift of the SP band wavelength shows a regular dependence on the refractive index of the medium, the extinction

(53) Yu, Y. Y.; Chang, S. S.; Lee, C. L.; Wang, C. R. C. *J. Phys. Chem. B* **1997**, *101*, 6661–6664.
(54) Myroshnychenko, V.; Rodriguez-Fernandez, J.; Pastoriza-Santos, I.; Funston, A. M.; Novo, C.; Mulvaney, P.; Liz-Marzan, L. M.; de Abajo, F. J. G. *Chem. Soc. Rev.* **2008**, *37*, 1792–1805.
(55) Vaskevich, A.; Sehayek, T.; Rubinstein, I. *Anal. Chem.* **2009**, *81*, 2877–2883.
(56) Maxwell-Garnett, J. C. *Philos. Trans. R. Soc. London* **1904**, *203*, 385–420.

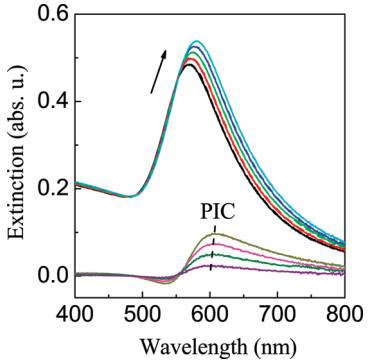

Figure 9. Transmission UV−vis spectra of a 7.5 nm Au island film evaporated on bare glass and annealed 10 h at 550 °C, measured in methanol−chloroform mixtures (1:0, 1:3, 1:1, 3:1, 0:1). Arrow indicates increase of the refractive index of the solution, from pure methanol (n = 1.327) to pure chloroform (n = 1.445). Each trace corresponds to two perfectly overlapping spectra obtained by changing the solution refractive index in an ascending and then descending order. Extinction difference curves (lower group) were obtained by subtracting the spectrum in pure methanol. The plasmon intensity change (PIC) was determined as the maximum of the extinction difference (dashed line).

intensity does not show a similar dependence. The present system, i.e., random Au island films prepared by evaporation/annealing, presents a highly regular response to change in the refractive index of the surrounding medium both in wavelength and in intensity change (Figure 9). This opens the possibility of the use of either or both parameters to evaluate the LSPR transducer response. Extinction changes can be determined at the SP band maximum; however, we[15,16,18] and others[4,9,26] found that maximal intensity changes are measured at wavelengths red-shifted from the SP maximum, as seen in Figure 9, bottom curves. We previously defined the maximum of the difference spectrum as the plasmon intensity change (PIC), indicating maximum sensitivity for intensity change measurement. It is noteworthy that the wavelength of the PIC is considerably less sensitive to change of the bulk refractive index than the wavelength of the SP maximum (Figure 9), as previously shown for adsorption of a self-assembled monolayer[16,18] and layer-by-layer assembly of multilayers.[15]

The bulk RIS is presented here as the SP wavelength shift (RIS_λ) and the PIC (RIS_{ext}). Respective experimental data are shown in Figures 10 and 11 and summarized in Table 2. Both the SP band wavelength and the PIC show a linear dependence on the refractive index of the medium in the measured RI range, with the slope (i.e., the RIS) generally increasing with the nominal thickness of the Au island films. A deviation is seen in the 10 nm high-temperature annealed Au island films, exhibiting lower RIS_{ext} values. The low-temperature annealed Au island films show a RIS_λ of 66−121 nm/RIU and a RIS_{ext} of 0.20−0.54 abs.u./RIU, while the RIS_λ and RIS_{ext} of the high-temperature annealed Au films are 93−153 nm/RIU and 0.23−0.81 abs.u./RIU, respectively. The Au island films studied here exhibit RIS values in the vicinity of previously reported results, e.g., evaporated Au island films and nanoparticles immobilized on flat substrates,

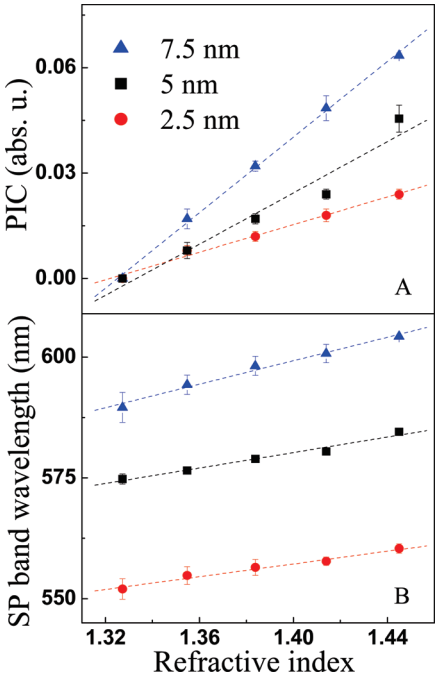

Figure 10. Dependence of the PIC (A) and SP band wavelength (B) on the refractive index of the bulk solution for Au films evaporated on silanized glass and annealed 20 h at 200 °C. Nominal thicknesses are indicated. The RIS_{ext} and RIS_λ are obtained as the slopes in A and B, respectively.

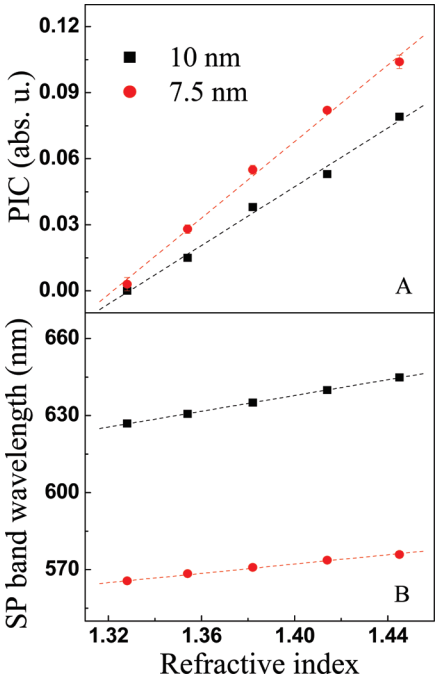

Figure 11. Dependence of the PIC (A) and SP band wavelength (B) on the refractive index of the solution for Au films evaporated on bare glass and annealed 10 h at 550 °C. Nominal thicknesses are indicated. The RIS_{ext} and RIS_λ are obtained as the slopes in A and B, respectively.

where the RIS approaches ca. 100 nm/RIU (RIS_λ) and ca. 1 abs. u./RIU (RIS_{ext}).[13]

Numerical calculations of optical properties of nanostructured metal films, using theoretical models and empirical correlations, provide the sensitivity of the LSPR band position for a variety of shape-defining

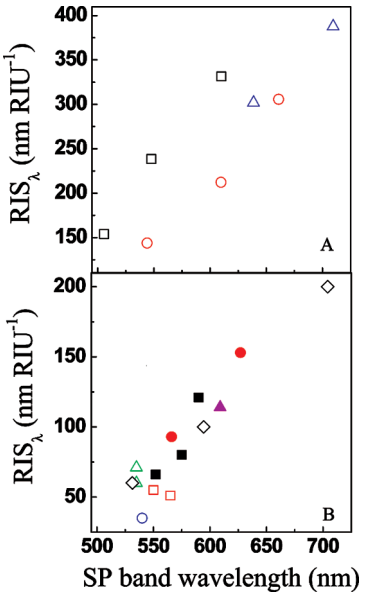

Figure 12. Relationship between the RIS$_\lambda$ of LSPR systems based on Au nanostructures and the wavelength of the SP band maximum, presented as calculated (A) and experimental (B) data. (A) Red circles: cylinders with an aspect ratio of 0.6, 1.5, and 2;[36] black squares: nanoparticles with a diameter of 20, 40, and 60 nm;[37] blue triangles: cylinders with a diameter of 20 nm and an aspect ratio of 2 and 2.6.[37] (B) Filled symbols present current data. Black squares: Au films evaporated on silanized glass and annealed 20 h at 200 °C; red circles: films evaporated on bare glass and annealed 10 h at 550 °C; magenta triangle: film evaporated on bare glass and annealed 10 h at 600 °C. Empty symbols present literature data. Red squares: Au island films on quartz;[58] blue circle: Au nanoparticles with a diameter of 12 nm immobilized on glass;[5] green triangles: Au nanoparticles with a diameter of 30 and 50 nm in solution;[27] black diamonds: Au nanodisks with an aspect ratio of 1, 3.5 and 7 on glass.[34] The SP band wavelength is given in methanol, $n = 1.327$ (current work) and in water, $n = 1.33$ (literature data).

parameters, furnishing (mainly qualitative) results useful for the optimization of LSPR transducers.[4,7,33,36,37,57] Semiempirical modeling of the RIS predicts a correlation between the SP band wavelength and the RIS$_\lambda$, also seen in direct calculations using discrete dipole approximation (DDA) (Figure 12A).[36,37] Figure 12B presents a compilation of experimental results obtained in the present study and literature results on various nanostructured Au films. The RIS$_\lambda$ increases approximately linearly with the shift in the position of the SP band maximum, in qualitative agreement with the theoretical models.[36] The results in Figure 12B, showing a common correlation behavior of different LSPR systems, suggest that the RIS can be estimated from the wavelength of the SP band maximum without detailed knowledge of the Au film morphology.

While the correlation presented in Figure 12B is quite useful in predicting general trends in the RIS, it should be considered with caution as additional factors should be taken into account, such as the nature of the metal island−substrate interface. The pronounced stability of high-temperature annealed Au island films is the result of partial embedding of the islands in the glass substrate.[19] However, the embedding reduces the RIS due to the decrease in the relative island surface exposed to the variable refractive index medium.[58,59] The Au islands in the films annealed at 550 and 600 °C show similar lateral dimensions, but the island height above the glass surface, measured by AFM cross-sectional profilometry, decreases with the increase in annealing temperature as a result of more extensive embedding (Table 1). The SP band of Au island films annealed at the higher temperature (600 °C) is red-shifted (Table 2), although the aspect ratio is practically unchanged (Table 1). The red shift is explained by the increase in the effective refractive index of the surrounding medium (air is replaced with glass). Therefore, in the case of the 550 and 600 °C annealed films, a red shift of the SP band is accompanied by a decrease in the RIS of the transducer (Table 2), contrary to the correlation shown in Figure 12. Hence, while the relationship in Figure 12 is generally valid, optimization of LSPR transducers should take into account the characteristics of the island−substrate interface.

Van Duyne, Schatz, and co-workers[31,60] introduced a dimensionless figure-of-merit (FOM) to compare the overall performance of LSPR transducers, defined as FOM = RIS$_\lambda$/fwhm. Values of the FOM for annealed Au island films are given in Table 2. The trend in the FOM values generally follows the RIS$_\lambda$, with the exception of the film annealed at 600 °C which is influenced by the extensive embedding. Of the films studied here, the best overall sensitivity (highest FOM) is obtained for the 10 nm Au island film annealed at 550 °C.

Conclusions

Preparation of Au island films by evaporation on glass substrates combined with postdeposition annealing affords a convenient and reproducible approach to the preparation of transducers for localized surface plasmon resonance (LSPR) spectroscopy. The issue of poor adhesion can be tackled either by evaporation on silanized glass followed by low-temperature (ca. 200 °C) annealing or by evaporation on bare glass followed by annealing at a high temperature (550 °C−600 °C), close to the glass-transition temperature of the substrate. High-temperature annealing results in wetting of the Au islands by the glass and partial embedding of the islands in the glass substrate, providing excellent stability of the morphology and optical properties. The mechanism of morphology evolution and island formation during annealing depends on the initial morphology of the unannealed film: Thinner films comprising separated islands undergo island coalescence and coarsening during annealing, while thicker, percolated films follow a dewetting course. Morphological study of films of different nominal thicknesses that underwent different annealing procedures shows that (i) islands formed by annealing of near-percolated films (7.5 nm nominal thickness) display larger scattering of the Feret diameter compared to islands formed by annealing

(57) Xu, H.; Kall, M. *Sens. Actuators, B* **2002**, *87*, 244–249.
(58) Meli, M.-V.; Lennox, R. B. *J. Phys. Chem. C* **2007**, *111*, 3658–3664.
(59) Novo, C.; Funston, A. M.; Pastoriza-Santos, I.; Liz-Marzan, L. M.; Mulvaney, P. *J. Phys. Chem. C* **2008**, *112*, 3–7.
(60) Sherry, L. J.; Chang, S. H.; Schatz, G. C.; Van Duyne, R. P.; Wiley, B. J.; Xia, Y. N. *Nano Lett.* **2005**, *5*, 2034–2038.

of either separated island or percolated films; (ii) Au islands formed by low-temperature annealing are close to prolate spheroids, while high-temperature annealed islands are single-crystalline faceted with top (111) surface; (iii) the aspect ratio of more than 90% of the islands in all the annealed films (except the low-temperature annealed 7.5 nm film) is less than 1.5. The low aspect ratio of the large majority of islands results in widening, rather than splitting, of the surface plasmon (SP) band. Hence, increase in the average aspect ratio is accompanied by an increase in the fwhm of the SP band.

The bulk refractive index sensitivity (RIS) of the SP extinction of low-temperature annealed Au island films (2.5, 5.0, and 7.5 nm nominal thickness) and high-temperature annealed Au island films (7.5 and 10 nm nominal thickness) was determined. The studied films show a linear dependence of the SP band wavelength and plasmon intensity change (PIC) on the refractive index (RI) of the surrounding medium in the measured RI range of 1.327−1.445. For the low-temperature annealed films, the values of the RIS_{λ} (SP wavelength shift) and RIS_{ext} (PIC) are in the range 66−121 nm/RIU and 0.2−0.54 abs. u./RIU, respectively, while the corresponding values for the high-temperature annealed films are in the range 93−153 nm/RIU and 0.23−0.81 abs.u./RIU. The bulk refractive index sensitivity RIS_{λ} shows a pronounced dependence on the SP band wavelength, i.e., the RIS_{λ} increases as the SP band is red-shifted. A deviation from this relationship is seen with the film annealed at 600 °C, where both the SP band position and the RIS are strongly affected by island partial embedding in the glass substrate.

The correlation between the SP band wavelength and the RIS may provide a useful tool for estimating the RIS of LSPR systems without detailed knowledge of the film morphology. It should be noted, though, that the structure of the island−substrate interface may also affect this general trend. The RIS results and relationships presented in this work may be useful in the design and optimization of Au island-based LSPR transducers.

Acknowledgment. Support of this work by the Gurwin Family Fund (Weizmann Institute) and by EU NEST project PROSURF, No. 028331, is gratefully acknowledged. This research is made possible in part by the historic generosity of the Harold Perlman family. We thank Dr. Ronit Popovitz-Biro (Weizmann Institute) for assisting with the cross-sectional TEM imaging and Dr. Tzipi Cohen-Hyams (Technion) for preparing the cross-sectional samples in the FIB microscope. The electron microscopy studies were conducted at the Irving and Cherna Moskowitz Center for Nano and Bio-Nano Imaging, Weizmann Institute of Science.

Supporting Information Available: Aspect ratio histograms for various Au island films (PDF). This material is available free of charge via the Internet at http://pubs.acs.org.